Monthly Notices
of the
ROYAL ASTRONOMICAL SOCIETY

Mon. Not. R. Astron. Soc. **410,** 2414–2421 (2011) doi:10.1111/j.1365-2966.2010.17615.x

Outflow rates in a black hole environment in presence of a dissipative standing shock

Chandra B. Singh[1] and Sandip K. Chakrabarti[1,2]★

[1]*Indian Centre for Space Physics, Chalantika 43, Garia Station Road, Kolkata 700084, India*
[2]*S. N. Bose National Centre for Basic Sciences, Salt Lake, Kolkata 700098, India*

Accepted 2010 August 28. Received 2010 July 10; in original form 2010 May 25

ABSTRACT

We find a self-consistent solution for the outflow rate from an accretion disc around a black hole. The centrifugal pressure dominated shock in a transonic accretion flow can act as a Compton cloud by emitting radiation in the form of hard X-rays. It is also the base of an outflow where considerable matter is ejected. We modify the Rankine–Hugoniot relationship in the accretion flow when the post-shock region suffers energy as well mass-loss. After connecting the post-shock solution in the disc with the sonic surface properties of the outflow, we obtain the ratio of the outflow rate and inflow rate $R_{\dot{m}}$ analytically. Our conclusions are (i) the outflow rate is at the most a few per cent of the inflow rate, (ii) the outflow is absent when the shock is relatively weak (more precisely, the compression ratio is less than about 2) and (iii) the outflow rate decreases with the increase of the energy loss at the post-shock region. Thus spectrally soft states will have lesser outflows.

Key words: black hole physics – shock waves – ISM: jets and outflows.

1 INTRODUCTION

Jets and outflows are the important components of black hole astrophysics. Indeed, even before black holes were discovered or even thought about, the powerful jets in the active galaxy M87 was discovered (Curtis 1918). Ever since the discovery of active galaxies and quasars in the 1960s and 1970s, powerful jets often were the only circumstantial evidences that a black hole may be residing at the galactic centre. In the case of stellar mass black hole candidates such as GRO J1655−40, GRS 1915+105, etc. where the mass is typically $\sim 10^{-9}$ times the mass of M87 (and hence these may be called nanoquasars), powerful jets are also observed which often move with almost the velocity of light.

Even after four decades of work on the origin, acceleration and collimation of jets, the jets and outflows are still not well understood. The magnetic field is ubiquitous, and intuitively it should play a major role in (i) transporting matter out of the disc, (ii) deciding the outflow velocity at the Alfvèn point and the Alfvèn speed is decided by the magnetic field strength. Furthermore, the inner disc being rotationally dominated, the field is expected to be mainly toroidal and thus when the toroidal field is buoyantly ejected out of the disc, the so-called 'hoop stress' would be of great assistance in collimating the flow. Thus, magnetic field should play a role in origin, acceleration and collimation of the outflows and jets. Blandford & Rees (1974), Blandford & Znajek (1977), Blandford & Payne (1982) and Camenzind (1990) among others have worked on the formation and collimation of jets by hydrodynamic and hydromagnetic processes. In these models, the power of the jet may directly come from the spin energy of the black hole or are driven by thermal, centrifugal or magnetic effects. On the other hand, in the transonic flow regime, the outflows are also solutions of the same equations [e.g. the approach of the solar wind solution of Parker (1958) is similar to the accretion solution of Bondi (1952)]. Here, the jets can use the thermal, magnetic or rotational energy at the base of the jet. Thus they may reach to infinity to achieve asymptotically a speed similar to either the hydrodynamic sound speed, or the Alfvèn speed, or the rotational speed that is present at the base, respectively. In the well-known Balbus–Hawley instability models, the magnetic turbulences are shown to increase the inflow rates and produce magnetized jets spontaneously (Krolik & Hawley 2007, and references therein).

Recently, it has been found that there is no evidence that the jets are powered by black hole spin (Fender, Gallo & Russell 2010), at least in the case of X-ray binaries and the authors speculate that this conclusion remains valid even for active galaxies and quasars. They conclude that there must be another parameter in the system which might be important for powering the jets. This convincing result immediately challenged the magnetized outflow models which depended on the spin energy. One other important parameter which might influence the outflows was discussed about more than a decade ago. It is the strength of the centrifugal pressure supported shock wave that is present in the flow for much of the parameter space. Chakrabarti (1985, 1986) postulated that just as

★E-mail: chakraba@bose.res.in

every outflow is formed from a boundary layer, the jets in the black hole systems should also be formed out of the CENtrifugal pressure dominated BOundary Layer or CENBOL which is nothing but the subsonic region between the inner critical point and the centrifugal force supported shock front in an accretion flow (Chakrabarti 1989, hereafter C89; Molteni, Langafame & Chakrabarti 1994). Only difference is that in the case of a star, the thickness of the boundary layer is very small compared to the radius of the star, but the width of the CENBOL could be typically the 10–20 times the size of the black hole. Incidentally, this region, in the absence of the radial velocities is known as the thick accretion disc. The physics behind its formation is roughly this: the centrifugal force grows as λ^2/r^3 while the gravitational force grows as $1/r^2$ (λ and r being the specific angular momentum and radius of the flow). As a result, for a given specific angular momentum, the centrifugal force may become dominant and slow down the matter by forming a shock. This very stable region is created due to piling up of matter behind the centrifugal barrier. In the post-shock region, the flow becomes hot. Chakrabarti & Titarchuk (1995) showed that this region also behaves as the Compton cloud which processes soft (low-energy) photons and emits hard (high-energy) photons. Chakrabarti (1998, 1999) subsequently proposed that the entire outflow is produced by the CENBOL and outflow rate directly depends on the compression ratio $R = \Sigma_+/\Sigma_-$ of the shock itself, where Σ is the integrated density of the flow in the pre-shock (marked with subscript '$-$') and post-shock (marked with subscript '$+$') region. This work was subsequently extended by adding angular momentum (Das et al. 2001) to this flow and a similar conclusion was reached. In particular, it was shown that when the shock is very weak ($R \sim 1$) or very strong ($R \sim 4$–7), the ratio of the outflow rate to the inflow rate $R_{\dot{m}}$ is lower, but when the shock strength is intermediate (say $\sim$2–3) $R_{\dot{m}}$ is very high and could be $\sim$0.2 or more. Two effects are major in determining the outflow rates: (i) the area of the CENBOL which increases with the shock location and (ii) the temperature of the CENBOL which decreases with the shock location. Since these two effects are opposite to each other, the effect is maximum when the CENBOL is of intermediate size. Fukumura & Kazanas (2007) extended the work of Das & Chakrabarti (2001). However, they included explicitly the loss of specific angular momentum as well. Since we are considering axisymmetric system, the loss of angular momentum is implicitly taken care of along with the mass-loss, and we do not consider such a loss separately. In any case, it was also established that the shock driven outflow is significant. Becker, Das & Le (2008) while concluding that the shocks are essential for driving outflows, showed that dissipative flows are perhaps more efficient in this regard. One of the examples that the base of the jet is really at most a few tens of Schwarzschild radii came from radio observation of M87 (Junor, Biretta & Livio 1999). It appears that the entire base is no more than $\sim$50 Schwarzschild radii, in agreement with the jet–disc connection hypothesis via a shock wave.

Since the hard radiation as well as jets and outflows are produced at the CENBOL itself, one would wonder whether the CENBOL itself would survive the loss of energy or it will collapse. Recently, Das, Chakrabarti & Mondal (2010) addressed this issue in great detail and they came to the conclusion that the parameter space of the flow which forms CENBOL shrinks in presence of dissipation. However, the region still remains sufficiently significant. They also found that for a given initial set of flow parameters, there is an upper limit of energy dissipation beyond which shock solution is not possible. This conclusion is very important, since according to Chakrabarti & Titarchuk (1995) also, the emission of hard photons stops when the accretion rate of the Keplerian disc (i.e. intensity of soft photons injected into the CENBOL) is increased. Thus, enhanced cooling, that is, dissipation in CENBOL, removes the CENBOL altogether. This purely theoretical exercise directly points to the fact that there should be a strong correlation between the spectral states and outflows. Simply put, in a soft state, the shock would be weak or absent and so is the outflow. In a hard state, the shock would be very strong but the outflow will be continuous, but not necessarily profuse. In an intermediate state, the shock strength would be intermediate, and but the outflow is profuse and take part in Comptonization process. As a result, the outflow may be blobby. These aspects of jet–disc connection and their ramifications are already in the literature (Chakrabarti 1999, hereafter C99; Chakrabarti & Nandi 2000) at least a decade ago.

In this paper, we follow the methodology of C99, Das et al. (2001, 2010) to compute the outflow rates in presence of energy as well as mass dissipations. Our goal is to have the most realistic hydrodynamical model with the outflow rate is self-consistently computed from the inflow rate where dissipation would be put in. In future, these solutions would be used to compute the spectral properties of the flow. In the next section, we will present the governing equations which we plan to solve. We consider three models of dissipation of the flow at the shock. We obtain the modified form of Rankine–Hugoniot relation in presence of energy dissipation and mass-loss from the post-shock region. In Section 3, we will present and discuss the results. In Section 4, we will present the concluding remarks.

2 GOVERNING EQUATIONS AND SHOCK CONDITIONS

We consider axisymmetric matter accreting on the equatorial plane of a Schwarzschild black hole. The geometry of our system is shown in Fig. 1. The centrifugal pressure forces the matter to have a standing shock at a distance governed by the Rankine–Hugoniot condition. At the CENBOL, the flow may lose $\Delta\mathcal{E}$ energy per unit gram and $\dot{M}_J$ gram of matter per second.

Space–time around the black hole is described by the Paczyński–Wiita pseudo-Newtonian potential $\phi = \frac{GM_{\rm BH}}{r-2GM_{\rm BH}/c^2}$ (Paczyński & Wiita 1980), where $M_{\rm BH}$ is the mass of the black hole and G, c are the gravitational constant and velocity of light, respectively. Here, r is the radial distance from the origin of the coordinate in which the black hole is placed at the centre. We use the geometric units in which the length, time and velocity scales are measured in units of $2GM_{\rm BH}/c^2, 2GM_{\rm BH}/c^3$ and c, respectively. In future, we use r to denote non-dimensional distance, ϑ and a to denote the non-dimensional radial velocity and adiabatic speed of sound, respectively. In accretion or outflow, we assume that the viscous stress is negligible so that matter moves with a constant specific angular momentum. In this case, the radial momentum equation for a non-dissipative flow in vertical equilibrium is given by (Chakrabarti 1989)

$$\vartheta\frac{\mathrm{d}\vartheta}{\mathrm{d}r} + \frac{1}{\rho}\frac{\mathrm{d}P}{\mathrm{d}r} - \frac{\lambda^2}{r^3} + \frac{1}{2(r-1)^2} = 0. \tag{1}$$

Integrating this, we obtain the conserved specific energy of the flow,

$$\mathcal{E} = \frac{1}{2}\vartheta^2 + na^2 + \frac{\lambda^2}{2r^2} - \frac{1}{2(r-1)}, \tag{2a}$$

where n is the polytropic index of the inflow and λ is the specific angular momentum. In equation (1), P and ρ are the thermal pressure and the density, respectively, ϑ is the infall velocity and $a = \sqrt{(\gamma P/\rho)}$ is the adiabatic sound speed. The mass conservation

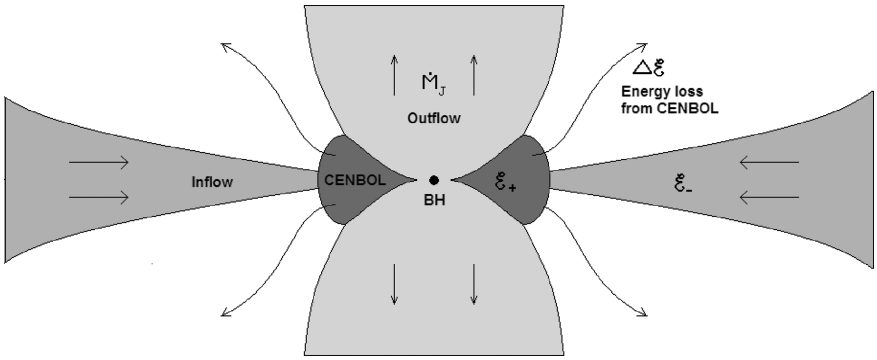

Figure 1. A cartoon diagram of the system under consideration. The axisymmetric accretion flow with specific energy $\mathcal{E}_-$ forms a centrifugal pressure supported boundary layer or CENBOL where the Rankine–Hugoniot condition is satisfied. At the CENBOL, the flow loses an energy of $\Delta\mathcal{E}$ per unit gram and $\dot{M}_J$ matter in the outflow.

equation is given by

$$\dot{M} = \Theta_i r h(r) \rho. \tag{2b}$$

Here Θ_i is solid angle subtended by the inflow. It is useful to rewrite this equation in terms of ϑ and a in the following way:

$$\dot{\mathcal{M}} = \vartheta a^q f(r), \tag{3}$$

where $q = (\gamma + 1)/(\gamma - 1)$. The functional form $f(r) = r^{3/2}(r - 1)$ is obtained by assuming the vertical equilibrium. Here, $\dot{\mathcal{M}}$ is the entropy accretion rate (C89) which is conserved (as $\dot{M}$) when is flow is ideal. However, in presence of shocks, where entropy is generated, $\dot{\mathcal{M}}$ will change.

2.1 Shock conditions in presence of energy loss and outflow

As the flow moves closer to the black hole, and the centrifugal force grows, at some point, the supersonic flow may become subsonic at the shock front (C89; Nobuta & Hanawa 1994). It becomes supersonic again after passing through the inner critical point (C89). The cooling of electrons takes place in the post-shock region through inverse Comptonization and is likely to be very important within a distance dr inside the shock where the optical depth is around unity. For simplicity, we assume that the entire energy dissipation takes place right at the shock itself. Thus, instead of the energy conservation condition at the shock, namely

$$\mathcal{E}_+ = \mathcal{E}_-,$$

we employ

$$\mathcal{E}_+ = \mathcal{E}_- - \Delta\mathcal{E} \tag{4a}$$

to allow a loss of energy per gram by $\Delta\mathcal{E}$ at the post-shock region. Similarly, instead of using the baryon number conservation,

$$\dot{M}_+ = \dot{M}_-,$$

we will use

$$\dot{M}_+ = \dot{M}_-(1 - R_{\dot{m}}). \tag{4b}$$

The pressure balance condition, where the sum of thermal pressure and ram pressure must match on the both sides of the shock (Landau & Lifshitz 1959), remains the same as in a non-dissipative flow, i.e.

$$W_+ + \Sigma_+ \vartheta_+^2 = W_- + \Sigma_- \vartheta_-^2. \tag{4c}$$

(We used subscripts '−' and '+' to refer, respectively, to quantities before and after the shock.) Here $\Delta\mathcal{E}$ and $R_{\dot{m}}$ refer to energy loss and ratio of the outflow rate and the inflow rate, respectively. W and Σ denote the pressure and the density, integrated in the vertical direction (see e.g. Matsumoto et al. 1984).

For the sake of concreteness, we can model $\Delta\mathcal{E}$ in three different ways.

(A) Since the dissipation is expected to be mostly through thermal Comptonization (Chakrabarti & Titarchuk 1995), it is assumed that the energy dissipation in the post-shock region reduces the temperature of the flow and the loss of energy is proportional to the temperature difference between the post-shock and the pre-shock flows, i.e.

$$\Delta\mathcal{E} = fn\left(a_+^2 - a_-^2\right)$$

(Das et al. 2010), where f is the fraction of thermal energy difference that is lost, and n is the polytropic constant.

(B) In case when bremsstrahlung is more important than the thermal Comptonization, the loss of energy would be average of the energies in the pre- and post-shock flows. We then obtain

$$\Delta\mathcal{E} = fn\frac{\left(a_+^2 + a_-^2\right)}{2}.$$

(C) In case the thermal energy of the pre-shock region is much smaller as compared to that of post-shock region, both of the above models reduce to

$$\Delta\mathcal{E} = fna_+^2.$$

When inverse Comptonization cools the electrons, it is the post-shock region that gets cooled. So in that respect model (C) is perhaps more realistic than model (A). However, model (C) allows the post-shock region to be cooler than the pre-shock flow by strong cooling effects, while in model (A) the post-shock region cannot be cooler than the pre-shock region.

We assume that the flow is in vertical equilibrium and thus use the sonic point analysis same as in C89. The radial velocity and the sound speed at the critical point is obtained from

$$\vartheta_c^2(r_c) = \frac{2}{\gamma + 1} a_c^2(r_c), \tag{5a}$$

$$a_c^2(r_c) = \frac{(\gamma + 1)(r_c - 1)}{r_c^2}\frac{\left(\lambda_k^2 - \lambda^2\right)}{(5r_c - 3)}, \tag{5b}$$

where

$$\lambda_k = \frac{r_c^3}{2(r_c - 1)^2},$$

is the Keplerian angular momentum per unit mass. The subscript 'c' denotes quantities at the critical point. In the vertical equilibrium

model the Mach number ϑ_c/a_c at the critical point is given by

$$M_c = \sqrt{\frac{\gamma+1}{2}}\frac{\vartheta_c}{a_c}.$$

For studying the shock solutions in terms of the flow parameters, we write the equations (4a), (3) and (4c) in terms of the Mach number $M = \vartheta/a$ of the flow,

$$\frac{1}{2}M_+^2 a_+^2 + \frac{a_+^2}{\gamma-1} + \Delta\mathcal{E} = \frac{1}{2}M_-^2 a_-^2 + \frac{a_-^2}{\gamma-1}, \tag{6a}$$

$$\dot{\mathcal{M}}_+ = M_+ a_+^{\nu} f(r_s), \tag{6b}$$

$$\dot{\mathcal{M}}_- = M_- a_-^{\nu} f(r_s), \tag{6c}$$

$$\frac{a_+^{\nu+1}\dot{M}_+}{\dot{\mathcal{M}}_+}\left[\frac{2\gamma}{3\gamma-1}+\gamma M_+^2\right] = \frac{a_-^{\nu+1}\dot{M}_-}{\dot{\mathcal{M}}_-}\left[\frac{2\gamma}{3\gamma-1}+\gamma M_-^2\right], \tag{6d}$$

where $\nu = (3\gamma-1)/(\gamma-1)$ and r_s is the location of the shock.

Using equations (6a)–(6d) one obtains the following equation relating the Mach numbers of the flow at the shock:

$$C = \frac{\left[\frac{2}{M_+}+M_+\left(\frac{2n+3}{n}\right)\right]^2[1-R_{\dot{m}}]^2}{\left[\frac{M_+^2}{2}+n\right]} = \frac{\left[\frac{2}{M_-}+M_-\left(\frac{2n+3}{n}\right)\right]^2}{\left[\frac{M_-^2}{2}+n-\frac{\Delta\mathcal{E}}{a_-^2}\right]}. \tag{7}$$

In our case, a sub-Keplerian flow with a positive energy will pass through the outer critical point and if the relation in equation (7) is satisfied, a standing shock may form.

In case there is no energy loss or mass-loss during the shock transition, then equation (7) reduces to

$$C = \frac{\left[\frac{2}{M_+}+M_+\left(\frac{2n+3}{n}\right)\right]^2}{\left[\frac{M_+^2}{2}+n\right]} = \frac{\left[\frac{2}{M_-}+M_-\left(\frac{2n+3}{n}\right)\right]^2}{\left[\frac{M_-^2}{2}+n\right]},$$

which is a familiar expression for a non-dissipative flow with no mass-loss (C89).

On further analysis, M_+ can be found by using the following expression:

$$AM_+^4 + BM_+^2 + CM_+ = 0,$$

where

$$A = 2(\gamma-1)(3\gamma-1)^2(1-R_{\dot{m}})^2 - C(\gamma-1),$$

$$B = 8(\gamma-1)(3\gamma-1)(1-R_{\dot{m}})^2 - 2C,$$

$$C = 8(\gamma-1)(1-R_{\dot{m}})^2.$$

M_- can be evaluated using this relation after using equations (3) and (6a):

$$M_-^2 = \frac{\left(\frac{\dot{\mathcal{M}}_+}{\dot{\mathcal{M}}_-}\frac{M_-}{M_+}\right)^{1/4}\left[2+(\gamma-1)M_+^2\right]-2}{(\gamma-1)} + \frac{2\Delta\mathcal{E}}{a_-^2}.$$

2.2 Outflow rate from inflow rate

In the pre-shock region, the matter is cooler. Assuming $\mathcal{E} \sim 0$ (freely falling condition) and $a \sim 0$ (cool gas) in presence of angular momentum, matter will fall with a velocity

$$\vartheta(r) = \left[\frac{1}{r-1}-\frac{\lambda^2}{r^2}\right]^{1/2}. \tag{8}$$

At the shock $r = r_s$, i.e. the boundary of the CENBOL, the compression ratio can be computed from the mass conservation equation and is given by

$$R = \frac{\Sigma_+}{\Sigma_-} = \frac{h_+(r_s)\rho_+(r_s)}{h_-(r_s)\rho_-(r_s)} = \frac{\vartheta_-}{\vartheta_+}. \tag{9}$$

To have an analytical expression of the outflow in terms of the known flow parameters, namely the specific energy, the angular momentum and the energy dissipation factor f, we need to make a few approximations.

First, we assume that in the pre-shock region, the thermal pressure is small in comparison to the ram pressure. Thus using equation (4c), we get

$$W_+(r_s) = \frac{R-1}{R}\Sigma_-(r_s)\vartheta_-^2(r_s). \tag{10}$$

The isothermal sound speed C_s in the post-shock region is obtained from

$$C_s^2 = \frac{W_+}{\Sigma_+} = \frac{R-1}{R^2}\vartheta_-^2 = \frac{1}{f_0}\left[\frac{r_s^2-\lambda^2(r_s-1)}{r_s^2(r_s-1)}\right], \tag{11}$$

where $f_0 = R^2/(R-1)$. At the CENBOL, the adiabatic sound speed is $a_s^2 = \gamma C_s^2$. Matter is thermally driven from the CENBOL towards the axis in the form of jet. One can assume that in between the CENBOL and the critical point z_c of the outflow the matter remains isothermal (C99) since the matter is practically in a heat bath, being surrounded by CENBOL. In an adiabatic flow with an equation of state $P = K\rho^{\gamma}$ (where K is a constant and a measure of entropy), one obtains the ratio of the density at the critical point and the density at the CENBOL as

$$\frac{\rho_c}{\rho_s} = \left[\frac{a_c^2}{a_s^2}\right]^n. \tag{12}$$

The outflow rate is given by

$$\dot{M}_o = \Theta_o\rho_c\vartheta_c z_c^2, \tag{13}$$

where Θ_o is the solid angle subtended by the outflow. From these relations and assuming $z_c - 1 \sim z_c$, and following the steps as in C99 and Das et al. (2001), one obtains the ratio of the outflow to the inflow rate as

$$R_{\dot{m}} = \frac{\Theta_o}{\Theta_i}\frac{\left[\frac{2n+1}{2n}\left(\frac{1}{5z_c}-\frac{2\lambda^2}{5z_c^2}\right)\right]^{(2n+1)/2}}{\left[\frac{(n+1)(R-1)}{nR^2}\left(\frac{1}{r_s-1}-\frac{\lambda^2}{r_s^2}\right)\right]^n} \times R\sqrt{\frac{2n}{2n+1}}\left[\frac{1}{r_s-1}-\frac{\lambda^2}{r_s^2}\right]^{-1/2}\left(\frac{z_c}{r_s}\right)^2. \tag{14}$$

Here, Θ_o and Θ_i are the solid angles subtended by the outflow and inflow, respectively. We have used $n = 3$ for a relativistic flow.

In C99, where the CENBOL was assumed to be spherical and angular momentum and dissipation of energy were assumed to be negligible, the ratio $R_{\dot{m}}$ was a function of geometry of the inflow and outflow as the compression ratio R. However, in this case, neither the injected energy nor the injected matter remains in the disc. As a result, the expression for $R_{\dot{m}}$ is complex (equation 14).

Our interest will be to obtain $R_{\dot{m}}$ self-consistently. The steps involved include (i) choice of the model of dissipation (Models A, B or C), (ii) choice of the fraction f of the injected energy and the (iii) injected energy and angular momentum themselves. After this we follow the procedure of C89 to obtain first a non-dissipative solution. Using that as our first guess, we iterate to obtain the shock location, shock strength, outflow rate, etc. through convergence of the code. Our results are presented in the next section.

3 RESULTS

In order to show the typical shock transitions in three models, we compute the energy and the entropy accretion rates at the sonic or critical points. In Figs 2(a)–(c), the specific energy of accretion flow is plotted against entropy accretion rate for a specific angular momentum of $\lambda = 1.74$ and $\gamma = 4/3$ for (a) Model (A), (b) Model (B) and (c) Model (C), respectively. In (a), the dashed line a_1a_2 represents the shock transition without any energy loss and is an ideal shock transition where energy of the accretion flow across the transition remains the same. In this case, the entropy accretion rate $\dot{\mathcal{M}}$ increases after the shock transition. However, in presence of radiative cooling, it is not necessary that the entropy has to increase, since radiated entropy could be more compared to the generated entropy at the shock. As a result, the entropy accretion rate may go down. a_3a_4 represents the shock transition in which there is an energy loss with $f = 0.3$ and yet, the post-shock entropy accretion rate is greater than pre-shock entropy accretion rate (i.e. $\dot{\mathcal{M}}_+ > \dot{\mathcal{M}}_-$). On the other hand, if we start with a different energy, we get a shock transition a_5a_6, where the same fractional energy loss of $f = 0.3$ occurs. However, in this case, the post-shock entropy accretion rate is lesser than the pre-shock accretion rate (i.e. $\dot{\mathcal{M}}_+ < \dot{\mathcal{M}}_-$).

In Fig. 2(b), we plot the corresponding cases by $a_1'a_2'$ ($f = 0$), $a_3'a_4'$ ($f = 0.07$) and $a_5'a_6'$ ($f = 0.07$) and in Fig. 2(c), we plot the corresponding cases by a_1a_2 ($f = 0$), $a_3''a_4''$ ($f = 0.06$) and $a_5''a_6''$ ($f = 0.06$), respectively.

In Figs 3(a)–(c), we plot the variation of $R_{\dot{m}}$ as a function of the compression ratio R for different fractions of energy loss. The flow angular momentum has been kept fixed at $\lambda = 1.82$. $\gamma = 4/3$ is chosen throughout. In Figs 3(a)–(c), we show results of Models (A), (B) and (C), respectively. f is marked on the curves. In all the cases, we note that $R_{\dot{m}}$ decreases with increase in the fraction f, be it the difference in post-shock and pre-shock thermal energy (Model A), the average of the two thermal energies (Model B) or the thermal energy of the post-shock region itself (Model C). In

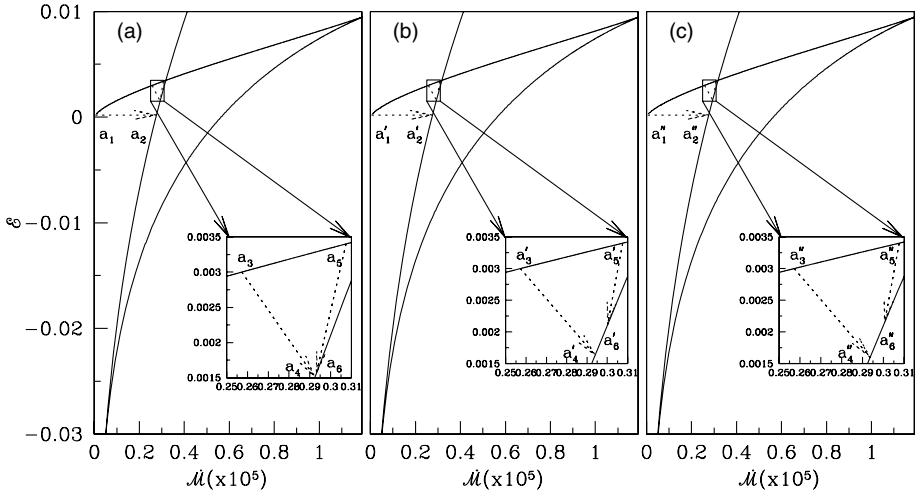

Figure 2. Energy $\mathcal{E}$ as a function of entropy accretion rate $\dot{\mathcal{M}}$ corresponding to different models of energy loss: (a) Model (A); (b) Model (B) and (c) Model (C). The shock transitions are shown with dashed lines. See the text for details.

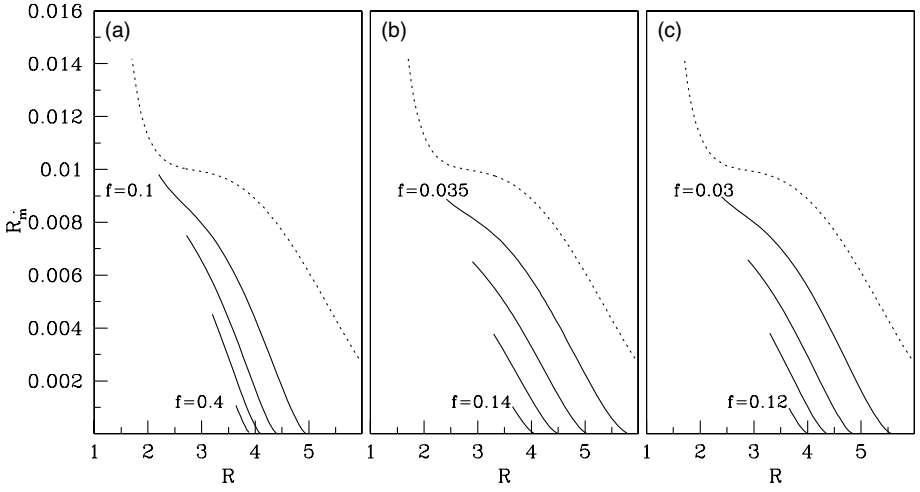

Figure 3. Variation of $R_{\dot{m}}$ as a function of compression ratio R for different models of energy loss: (a) Model (A): f varies from 0.1 (top curve) to 0.4 (bottom curve) with an interval of 0.1; (b) Model (B): f varies from 0.035 (top curve) to 0.14 (bottom curve) with an interval of 0.035; (c) Model (C): f varies from 0.03 (top curve) to 0.12 (bottom curve) with an interval of 0.03. The dashed curve in all the cases represents the outflow rates without any energy dissipation. Note that the outflow rate goes down when the compression ratio increases. Below a certain compression ratio, depending on the energy loss, no self-consistent solution exists. Also, the higher the fractional loss is, the lower is the outflow rate, as the post-shock flow loses thermal drive.

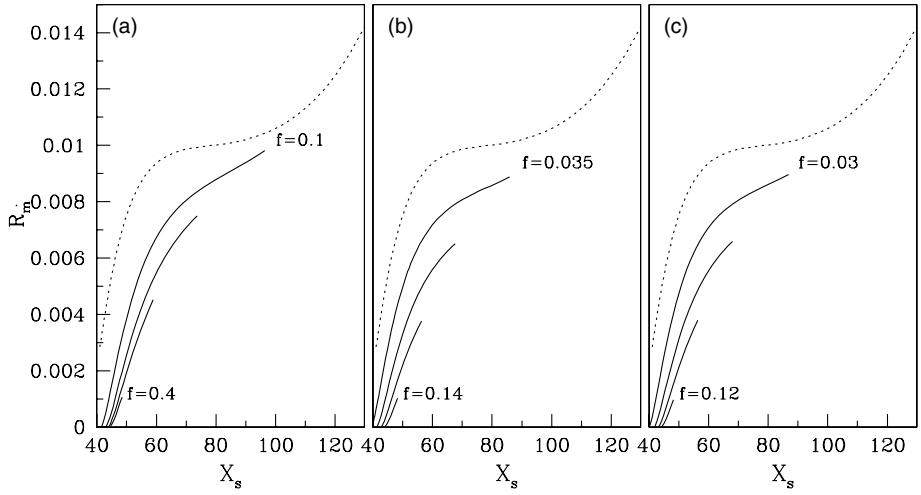

Figure 4. (a–c) Same as in Figs 3(a)–(c), but the variation of $R_{\dot{m}}$ as a function of shock locations X_s is plotted. In all the cases, we find that the flow with lowest factional energy dissipation can have shocks closest to the black holes. The dashed curve represents the outflow rates without any energy dissipation.

all the cases, $R_{\dot{m}}$ decreases as we increase R. This is because, for higher value of R, the shock moves inward. As a result, though the CENBOL temperature goes up and the CENBOL surface (i.e. the cross-sectional area of the base of jet) decreases. Hence the outflow rate also goes down. Below a certain R, no self-consistent solution is possible. Unlike the case of non-dissipative solutions of outflow rates, where $R_{\dot{m}}$ peaked at an intermediate R (C99), we find here that the solutions for weaker R is totally missing. This implies that when the compression ratio is smaller, no CENBOL is capable of losing energy and mass. This is consistent with the fact that the softer states which do not have hot Compton clouds, will not have outflows, a fact corroborated by all the observations (see Fender et al. 2010, and references therein). Instead of the compression ratio, if we plot $R_{\dot{m}}$ as a function of the shock strength M_-/M_+, we will have a similar result.

In Figs 4(a)–(c), we show the variation of $R_{\dot{m}}$ as a function of shock locations X_s (actually X_{s_3} in the notation of C89) for different values f. The flow parameters are the same as in Figs 3(a)–(c). First of all, it is observed that the outflow rate decreases as the shock location is going down. This is expected since in this model the base of the outflow is the CENBOL itself. It is also observed that for a particular value of $R_{\dot{m}}$, the shocks have to be located at a larger distance if the fractional dissipation is higher. In Models (B) and (C) results, we note that even when the loss fraction f is reduced, the shock location is not close to the black hole.

In Figs 5(a)–(c), $R_{\dot{m}}$ has been plotted as a function of $\mathcal{E}$ of the post-shock flow. It is clear that higher outflow rates are possible for flows which start with higher specific energy. Lower energy flows are capable of higher fraction of energy losses but the outflow rates are lower in these cases. The flow parameters are same as in Figs 3(a)–(c).

In Figs 6(a)–(c), the relationship between the shock location X_s is plotted against the compression ratio R. The flow parameters are the same as in Figs 3(a)–(c). A very important conclusion we draw is that as the energy loss increases, the shock location shifts towards the black hole. This is because the energy loss causes the post-shock region to cool down. Thus the Rankine–Hugoniot condition can be satisfied only if the shock shifts to higher thermal pressure. However, beyond a certain amount of energy loss in the CENBOL, a stable shock cannot exist. Considering the flow parameter to be

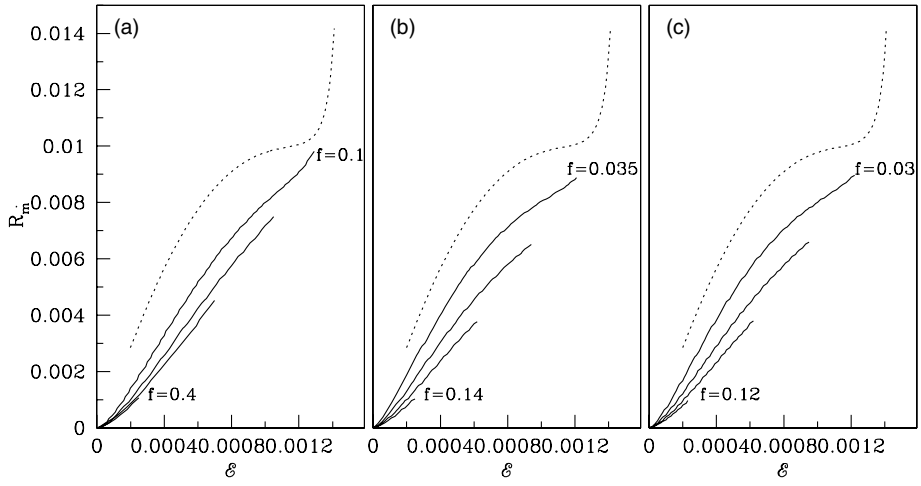

Figure 5. (a–c) Ratio of the outflow and the inflow rates $R_{\dot{m}}$ as a function of specific energy, $\mathcal{E}$, of the post-shock flow for all the three models of dissipation as in Figs 3(a)–(c). In all the cases, we find that the flow with the highest CENBOL energy can have the highest outflow rates. The dashed curve represents the outflow rates without any energy dissipation.

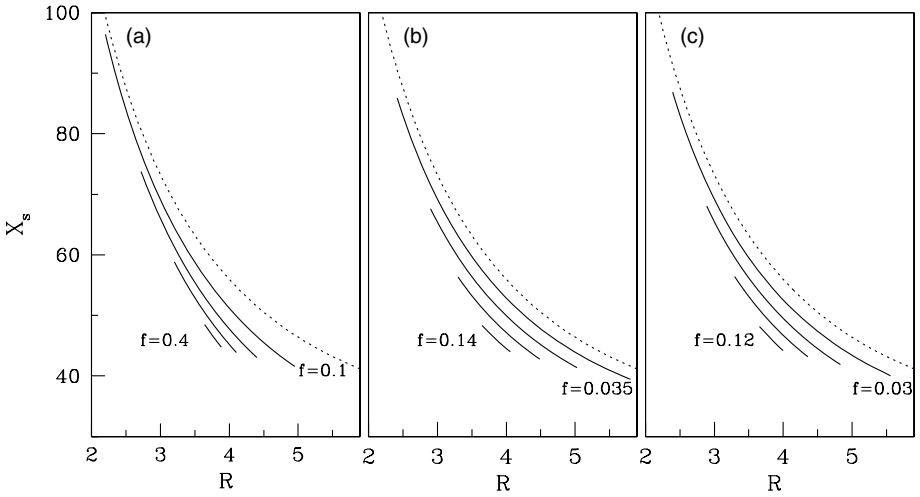

Figure 6. (a–c) Shock location X_s as a function of compression ratio R in all the three models as in Figs 3(a)–(c). The dashed curve represents the shock locations without any energy dissipation.

$\lambda = 1.82$ and energy dissipation to be of the form of Model (A), i.e. $\Delta\mathcal{E} = fn(a_+^2 - a_-^2)$, the maximum allowed value of f for a standing shock to form is found to be 0.44. Similarly, for Models (B) and (C), the maximum allowed values of f are obtained as 0.16 and 0.13, respectively.

4 DISCUSSION AND CONCLUDING REMARKS

In C99, it was pointed out that since the transonic accretion flow is likely to have a centrifugal pressure supported shock wave, especially in harder states, the outflows may be thermally and centrifugally driven from the post-shock region. Subsequently, Das et al. (2010) found that the solutions continue to have shock waves even when the post-shock region has energy loss through various cooling processes. In this paper, we generalize this work even further and explore the possibility of formation of outflows in presence of dissipation of energy in the post-shock region. Thus this work is more complete and more realistic.

There are several differences between the nature of outflow solutions in the absence and presence of dissipation. In the case of no-dissipation, the outflow rate was possible even for very weak shocks. The ratio of outflow and inflow rates ($R_{\dot{m}}$) was found to be as high as 0.15–0.2. In the presence of dissipation and energy loss at the CENBOL, the outflow was no longer possible as the shock is weaker. Indeed, the self-consistent solution does not yield any result for a compression ratio below $\sim$2. Furthermore, the highest outflow rate, obtained from self-consistently obtained Mach number relationship is found to be not more than a few per cent. We also found a new set of solutions: in presence of cooling, in the post-shock flow, it is found that shock transitions are possible where the specific entropy be reduced at the shock transitions.

Understanding the origin, acceleration and collimation of outflows from an accretion is a long-standing problem. While it was earlier believed that the entire disc may be taking part to supply the most powerful radio jets, detailed analysis indicates that a Keplerian disc which is itself a bound system (with negative energy) may not be capable to supply and accelerate matter to a large distance (Chakrabarti & Bhaskaran 1992). Naturally, flows with positive Bernoulli's constant and with high entropy are more suitable in this regard. Keeping these in mind, it was postulated (C99) that the post-shock region which loses radiative energy may also be solely responsible for energetic outflows. The high-resolution imaging of the powerful jet in M87 does show that the base is not larger than a few tens of Schwarzschild radii (Junor et al. 1999) thereby lending a support to such a hypothesis. Furthermore, the results of Fender and his group (see Fender et al. 2010, and references therein) found evidences of strong relationship between the spectral states and the outflows and found no evidences that spin of a black hole is related to the outflows. They postulated that there must be other parameters responsible for luminosity of the jets. The solution of centrifugal force dominated shocks is weakly dependent on the spin of a black hole and we strongly believe that these shocks are responsible for the outflows.

We have purposely left out the magnetic fields from our consideration of computing the outflow rates. So far, there is no convincing proof that magnetic field plays any major role, though from the high and often superluminal asymptotic velocity it is natural to assume that the energy must be magnetic in nature. However, we believe that if present, the field must be dominated by the toroidal component and could contribute to the collimation of the jet.

There are several works in the literature which computes the outflow rates using numerical simulations. In Molteni et al. (1994), it was shown that for a non-dissipative flow, the outflow rate could be anywhere between 8 and 10 per cent of the inflow. However, when dissipation is added in the post-shock region, the outflow rate becomes lower. Our conclusions, which are totally drawn from analytical work, roughly agree with very complex recent simulation results using other disc models. Ohsuga et al. (2009) showed that depending on the disc model, the ratio of outflow to inflow rates could vary from $\sim$1 to $\sim$10 per cent.

ACKNOWLEDGMENT

The work of CBS is partly supported by ICTP Junior fellowship with the Indian Centre for Space Physics.

REFERENCES

Becker P., Das S., Le T., 2008, ApJ, 677, L93
Blandford R. D., Payne D. G., 1982, MNRAS, 199, 883
Blandford R. D., Rees M. J., 1974, MNRAS, 169, 395
Blandford R. D., Znajek R. L., 1977, MNRAS, 179, 433

Bondi H., 1952, MNRAS, 112, 195
Camenzind M., 1990, Rev. Modern Astron., 3, 234
Chakrabarti S. K., 1985, ApJ, 288, 1
Chakrabarti S. K., 1986, ApJ 303, 582
Chakrabarti S. K., 1989, ApJ, 347, 365 (C89)
Chakrabarti S. K., 1998, Indian J. Phys., 72(B), 183
Chakrabarti S. K., 1999, A&A, 351, 185 (C99)
Chakrabarti S. K., Bhaskaran P., 1992, MNRAS, 255, 255
Chakrabarti S. K., Nandi A., 2000, Indian J. Phys., 75(B), 1
Chakrabarti S. K., Titarchuk L. G., 1995, ApJ, 455, 623
Curtis H. D., 1918, Publ. Lick Obser., 13, 31
Das S., Chattopadhyay I., Nandi A., Chakrabarti S. K., 2001, A&A, 379, 683
Das S., Chakrabarti S. K., Mondal S., 2010, MNRAS, 401, 2053
Fender R. P., Gallo E., Russell D., 2010, MNRAS, 406, 1425
Fukumura K., Kazanas D., 2007, ApJ, 669, 85
Junor W., Biretta J. A., Livio M., 1999, Nat, 401, 891
Krolik J. H., Hawley J. F., 2007, in Antonelli L. A., Israel G. L., Piersanti L., Tornambe A., eds, AIP Conf. Ser. Vol. 924, The Multicolored Landscape of Compact Objects and their Explosive Origins. Am. Inst. Phys., New York, p. 801
Landau L. D., Lifshitz E. M., 1959, Fluid Mechanics. Pergamon Press, Oxford
Matsumoto R., Kato S., Fukue J., Okazaki A. T., 1984, PASJ, 36, 71
Molteni D., Langafame G., Chakrabarti S. K., 1994, ApJ, 436, 249
Nobuta K., Hanawa T., 1994, PASJ, 46, 257
Ohsuga K., Mineshige S., Mori M., Kato Y., 2009, PASJ, 61, L7
Paczyński B., Wiita P. J., 1980, A&A, 88, 23
Parker E. N., 1958, ApJ, 128, 664

This paper has been typeset from a TEX/LATEX file prepared by the author.